

See discussions, stats, and author profiles for this publication at: <https://www.researchgate.net/publication/231647044>

Influence of pH and Pyrenyl on the Structural and Morphological Control of Peptide Nanotubes

ARTICLE *in* THE JOURNAL OF PHYSICAL CHEMISTRY C · APRIL 2011

Impact Factor: 4.77 · DOI: 10.1021/jp1120788

CITATIONS

12

READS

34

8 AUTHORS, INCLUDING:



Tatiana Martins

Universidade Federal de Goiás

11 PUBLICATIONS 101 CITATIONS

SEE PROFILE



Fabio Furlan Ferreira

Universidade Federal do ABC (UFABC)

70 PUBLICATIONS 538 CITATIONS

SEE PROFILE



Jose Antonio Souza

Universidade Federal do ABC (UFABC)

46 PUBLICATIONS 331 CITATIONS

SEE PROFILE



Wendel A. Alves

Universidade Federal do ABC (UFABC)

66 PUBLICATIONS 510 CITATIONS

SEE PROFILE


Influence of pH and Pyrenyl on the Structural and Morphological Control of Peptide Nanotubes

Tatiana D. Martins,^{†,§} Márcia I. de Souza,^{†,‡} Bruno B. Cunha,[†] Pedro M. Takahashi,[†] Fabio F. Ferreira,[†] José A. Souza,[†] Eudes E. Fileti,[†] and Wendel A. Alves^{*,†,‡}

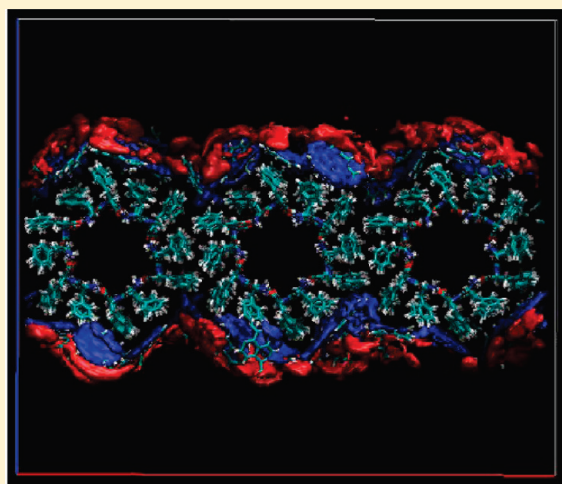
[†]Centro de Ciências Naturais e Humanas, Universidade Federal do ABC, 09210-170, Santo André, SP, Brazil

[‡]Instituto Nacional de Ciência e Tecnologia de Bioanalítica, 13083-970, P.O. Box 6154, Campinas, SP, Brazil

[§]Instituto de Química, Universidade Federal de Goiás, 74001-970, Goiânia, GO, Brazil

 Supporting Information

ABSTRACT: Using fluorescence spectroscopy techniques, the interaction of pyrenyl-1-carboxylic acid with diphenylalanine nanotubes and the effect of pH on the assembled nanostructures were studied. The nanotubes were doped with the fluorophore, and it was found that the fluorophore concentration affected the final structures. The nanotubes obtained at low pH are smaller than those obtained at neutral pH. The nanotubes self-arrange to produce microribbons at high pH values, and this behavior is quite distinct at high fluorophore concentrations, as shown by scanning electron microscopy (SEM), epifluorescence microscopy (EPM), and X-ray diffraction (XRD) measurements. These materials were placed onto glass and glass-modified ITO, and fluorescence spectroscopy data show that the ITO interacts with the nanotubes and that a radioactive energy-transfer process between pyrenyl moieties and ITO is favored. To gain insight into the interactions between nanotubes and pyrenyl at the molecular level, molecular dynamics simulations were carried out. The computational results show that the fluorophore doping absorbs strongly at the tube surface. Thus, surface functionalization of the nanotube was observed. The pyrenyl apolar group interacts with the tube, and its polar head is exposed to interactions with water molecules in the medium.



INTRODUCTION

Since the recognition of the natural self-assembly capability of peptides and their replication to obtain nanotubes *in vitro*,¹ several studies have been carried out for their potential application in nanotechnological processes. In these compounds, molecules self-assemble spontaneously, generating well-defined structures through noncovalent interactions under near-thermodynamic-equilibrium conditions. Such molecular self-assemblies rely on chemical and structural compatibilities because these interactions may involve hydrogen bonds or electrostatic, van der Waals, or various other interactions, resulting in integral and efficient supramolecular structures.²

Phenylalanine-containing polypeptides have amphiphilic properties that are responsible for their self-organization. They can self-assemble into a variety of morphologies, including micelles, nanorods, nanotubes, nanospheres, nanowires, and vesicular aggregates, depending on the preparation conditions, such as concentration, pH, and temperature.³ These fundamental properties are necessary for the fabrication of nanoscale functional structured materials that require novel physical, chemical, and electronic properties.^{3–5}

Investigations on the effect of pH on peptide self-assembly have^{4,6} revealed that, by adjusting the pH and the concentration of a peptide aqueous solution, a reversible reaction between the nematic gel phase and the isotropic fluid phase can occur. This responsive behavior is governed by the peptide amino acid portion, which enables a hierarchical assembly of β -sheets through chemical and structural complementarities. With this purpose in mind, control of the architecture is achieved by various methods,⁷ and a favored structure can be designed. New research has demonstrated that supramolecular structures based on organized assemblies of chromophores possess potential applications in nanotechnology, such as molecular electronics and light harvesting;⁸ these assemblies can be obtained by covalent linkages among the components or stabilized by weak interactions, such as electrostatic forces and dipole interactions. Manipulation of self-assembled structures is a promising alternative to nanofabrication technologies. The connection of such structures on solid surfaces

Received: December 20, 2010

Revised: March 29, 2011

Published: April 07, 2011

is a fundamental process for the development of molecule-based nanodevices.⁹

In this way, peptides are being modified physically and chemically, leading to stable materials with interesting new properties.¹⁰ Peptide compounds have been modified with chromophores to generate probes that permit new nondestructive methods of analysis and yield materials with optical responses,¹¹ although it is known that these probes can force the assembly of short peptides via π – π interactions between chromophores.¹²

In this work, we have demonstrated the influence of solution pH on the structural control of (L-Phe···L-Phe)-based polypeptides. Pyrenyl moieties were added as chromophoric probes to perform fluorescence spectroscopy studies of the obtained materials, and their effects on the nanostructure were also studied. Moreover, simulation studies on neutral nanotubes reveal the noncovalent functionalization of peptide nanotube walls with pyrenyl-1-carboxylic acid through an irreversible π – π stacking interaction. The results provide a full characterization of the structural and dynamic properties of this class of nanotubes and indicate interesting possibilities for the design of new devices.

■ EXPERIMENTAL DETAILS

Nanotube Preparation. Peptide nanotubes were prepared in controlled pH environments and doped with fluorophores for downstream fluorescence spectroscopy to explore their formation mechanism and determine the influence of pH on their final structures. To accomplish this goal, L-phenylalanine···L-phenylalanine (L-Phe···L-Phe) peptide nanotubes were prepared in distinct pH buffers (pH = 3, 7, and 10) and doped with fluorophores with well-known photophysical characteristics, such as 1-pyrene-carboxylic acid, a pyrenyl derivative. The fluorescent response was determined in a range of alcoholic solutions at distinct concentrations, which allowed the selection of solution characteristics that provided the best doping solution. The nanotubes were prepared in plastic flasks, on a glass surface, and on an indium tin oxide (ITO)-covered glass surface to provide information about any luminescent processes of the doped nanotube that could be influenced by the ITO.

Fluorophore solutions were prepared at a concentration of 10^{-5} mol L⁻¹ in dichloromethane for use as doping agents. The chosen fluorophore was 98% 1-pyrene-carboxylic acid, which was supplied by Sigma-Aldrich and used as received. Solutions at distinct concentrations and solvents were prepared to select the best doping solution, free of aggregation or excimer formation. UV/vis absorption, excitation, and fluorescence spectra were also obtained to determine the optimal conditions.

Peptide nanotubes were prepared in a plastic tube, into which 3 mg of L-Phe···L-Phe, also supplied by Sigma-Aldrich, was dissolved in a few drops of 1,1,1,3,3,3-hexafluoro-propanol (HFP). The fluorophore solution (500 μ L) was added to generate materials with 0.07% m/m of the fluorophore, followed by 500 μ L of pH 3 buffer to generate peptide nanotubes doped with a fluorescent compound having well-known photophysical characteristics. The same nanotube preparation methodology was employed using buffer solutions at pH 7 and pH 10 under the same conditions of fluorophore concentration, temperature, and material quantities. The same procedure was also used to prepare pyrenyl-diluted samples by adding 12.5 μ L of fluorophore solution instead of 500 μ L. The fluorophore concentration in the diluted samples was 0.002% m/m.

Next, the nanotubes were adsorbed onto a glass surface and an ITO-covered glass surface by adding 20 μ L of the L-Phe···L-Phe/fluorophore solution at each concentration and another 20 μ L of the buffer solution. All of the materials deposited on the surfaces were kept in a fume hood for 24 h to ensure solvent extraction and then kept in a vacuum flask. Finally, the materials were characterized by Fourier transform infrared (FTIR) spectroscopy and X-ray diffraction (XRD) and studied using steady-state fluorescence spectroscopy as well as epifluorescence (EPM) and scanning electron (SEM) microscopies.

Structural, Morphological, and Physical Characterization.

The XRD patterns of powdered samples were recorded at room temperature on a Rigaku Miniflex diffractometer using Cu–K α radiation (λ = 0.154 nm) in the 2θ range of 1.5–70° and operating at 30 mA and 40 kV. A scan rate of 1° min⁻¹ was used at room temperature. SEM images were obtained using a JEOL FEG-SEM JSM 6330F or JEOL LV-SEM microscope at the LME/LNLS (Laboratory of Electron Microscopy of the Brazilian Synchrotron Light Laboratory, Campinas, Brazil). The modified nanotubes adsorbed onto the glass and the ITO surfaces were characterized using UV/vis absorption spectra from a VARIAN 50 Scan spectrophotometer. Steady-state fluorescence measurements were performed using a PC1-ISS single-photon spectrofluorometer with a Xe arc lamp and 1 mm excitation and emission slits. The samples were positioned at an angle of 45° from the excitation slit, and the fluorescence was measured at an accurate angle. Excitation spectra were obtained by monitoring the emission at 420 nm and recorded in the range of 290–400 nm. Emission spectra were recorded with excitation at 330 nm and in the range of 350–500 nm. No emission of the excimer/aggregate fluorophore compounds was observed in this region. Fluorescence lifetimes were measured in a time correlated single photon counting (TCSPC) FL-900 Spectrophotometer, Edinburgh Analytical Instruments, that uses a pulsed hydrogen arc lamp, with a repetition of 40 kHz. The emission wavelength for the collection of counts was in the fluorescence maximum (λ_{em} = 390 nm), and excitation was performed at the absorption maximum of the pyrenyl moieties' spectra (λ_{em} = 350 nm). Solid samples were aligned at 45° to the incident radiation, and the emission was collected at a right angle from the front-face of the sample. Samples were sealed under vacuum to avoid oxygen suppression of fluorescence. The instrument response was determined using Ludox as a scatterer. At least 10⁴ counts were collected in the peak channel. Deconvolution of the lamp pulse was performed by nonlinear least-squares routines using the software supplied by Edinburg. The best fit was achieved when the χ^2 is close to 1. Epifluorescence microscopy was performed using a Leica Dm IRB inverted microscope with a HBO 100 W lamp and a 330–380 nm excitation filter. Fluorescence images were recorded using a SDC-311 ND Samsung camera and analyzed using Linksys software, v. 2.38. Objectives of 2.5, 10, 20, and 50 \times were used to acquire images. There was a 10-fold magnification of the image captured by the digital camera.

Computational Simulation Procedure. Computational simulation studies were performed to model the wall of the peptide nanotubes formed by tubular subunits of the L-Phe···L-Phe dipeptides in the presence of water. An investigation of the fluorophore adsorption process at the nanotube surface was necessary. The first atomic starting peptide coordinates were described by Görbitz.¹³ Recent investigations on the effect of water incorporation in the formation of dipeptide nanotubes and nanowires studied

by Kim et al.¹⁴ provided a better description of the system, because positional and torsional angles were taken into account. Thus, this crystal structure was considered as a starting model for the molecular dynamics simulations performed herein. The computational cell obtained for the doped system consisted of three juxtaposed tube units with a length of 5.46 nm (10 hexamers), forming a surface area of $5.46 \times 7.64 \text{ nm}^2$. This system was placed in a 6.50 nm high water/ion box. A similar box simulation, but without ions, was prepared in an identical fashion and used as the neutral reference system. Molecular dynamic (MD) simulations were carried out using GROMACS, version 4.5,¹⁵ and the Charmm27 force field.¹⁶ The TIP3P potential was used to describe the potential interaction of the water molecules.¹⁶ The system was investigated using the NPT ensemble in normal conditions ($T = 300 \text{ K}$ and $p = 1 \text{ bar}$ with periodic boundary conditions). As usual, the solute–solvent interactions were described using the Lennard-Jones and Coulomb potentials. Further details are given in the Supporting Information.

RESULTS AND DISCUSSION

The photophysical properties of pyrenyl-doped (L-Phe···L-Phe) nanotubes were studied, and steady-state and time-dependent fluorescence spectra were obtained for different preparation conditions, for example, different pH values, pyrenyl concentrations, and deposition surface. These data were correlated to the respective EPM and SEM images and XRD results to gain further insight into the morphological characteristics of the nanotubes. Spectral data for the fluorophore in solution were obtained for comparison.

Steady-state fluorescence spectra were obtained from the front face of the nanotube powder placed on a quartz substrate. Excitation was performed at 340 nm, and spectra were recorded from 350 to 500 nm. For all samples evaluated, spectra showed a maximum at 375 nm and another important peak at 390 nm; these peaks were assigned to the pyrenyl monomers. The spectra obtained are similar to those of the pyrenyl compound found in solution, but with a much poorer vibronic resolution. No structureless band at 450–500 nm, related to the presence of pyrenyl aggregates or an excimer, was observed (Figure 1).

Fluorescence lifetimes were obtained for solid-state samples from the front-face assembly. The data were fitted by a biexponential curve, which revealed two contributing fluorescent lifetimes. The first, which contributes to 80% of the total decay curve, is approximately 100 ns and is as expected for pyrenyl moieties, although these lifetimes can be very distinct for each sample. The second, which contributes to 20% of the total decay curve, is due to the emission of species that are separated from the monomer, indicating the presence of a small amount of aggregated species. Some fluorescent and morphological characteristics were modulated by the pH variation and pyrenyl concentration, as discussed below.

Effect of pH Changes. L-Phe···L-Phe nanotubes were formed by the addition of water to the peptide solution that already contained the fluorescent probe. Buffer solutions were added instead of pure water, and the formation of the nanotubes occurred at a very well-defined pH. Fluorescence spectra, lifetime measurements, and EPM and SEM images were recorded for the obtained nanotubes.

From the spectral data in Figure 1, some differences in the vibronic structure can be observed due to the protonation of the carboxyl group. At high pH, the first vibronic band is more

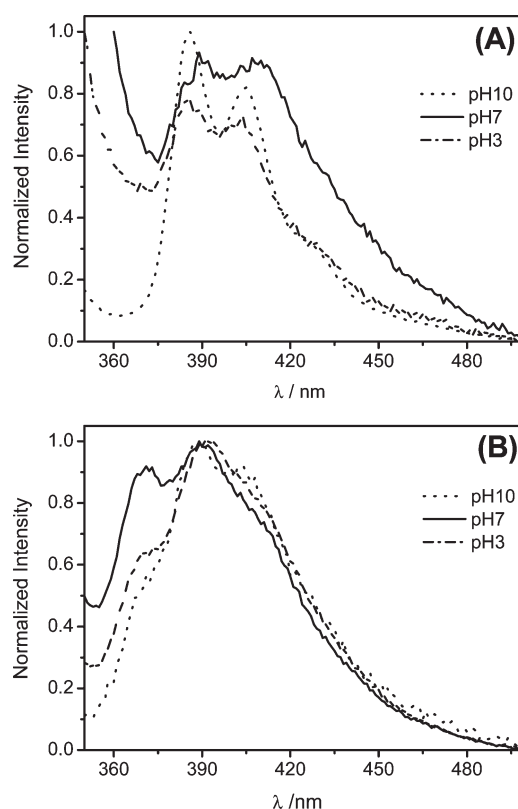


Figure 1. Fluorescence spectra of nanotubes formed with pyrenyl moiety concentrations of (A) 0.002% and (B) 0.07% m/m.

intense than the second one. At low pH, the intensity of the first band is less than that at high pH, and at neutral pH, these two bands are very close in intensity. These observations can be explained by the expectation that the carboxyl groups of the pyrenyl and the amino groups of the peptidic nanotube are protonated at lower pH, because the upper pH limit of 5.4 corresponds to the isoelectric point (pI) of diphenylalanine, where the net charge of diphenylalanine changes its sign.⁴ Thus, there is a less-effective electrostatic interaction between the components, and the van der Waals interaction between pyrenyl moieties is more prominent, leading to this self-absorption effect. At neutral pH, the amino groups of the fluorophore are protonated, but the carboxyl groups of the nanotube and pyrenyl moieties are not protonated; thus, the electrostatic interaction between the nanotubes and the fluorophore is still favored. At high pH, the carboxyl and amino groups of the peptide termination are deprotonated. There is a consequent decrease of electrostatic interactions because the repulsion interaction between the fluorophore and the nanotubes is predominant in this configuration. In fact, as shown by Tang et al., the overall negative surface charge of the Fmoc-diphenylalanine self-assembled fibrils increases in alkaline solutions from pH 7 to pH 10.¹⁷ This same behavior has been also demonstrated by Park et al., because the pH of the surrounding reaction mixture influences the net charge of diphenylalanine molecules; it also determines the net charge of the assembled nanowires.⁴ In the studied system, these effects are observed even when nanotubes are adsorbed on the surface of either glass or ITO, although some differences are detected.

In view of the clear effect of the controlled pH on the photophysical response of the fluorophore, it was expected that some

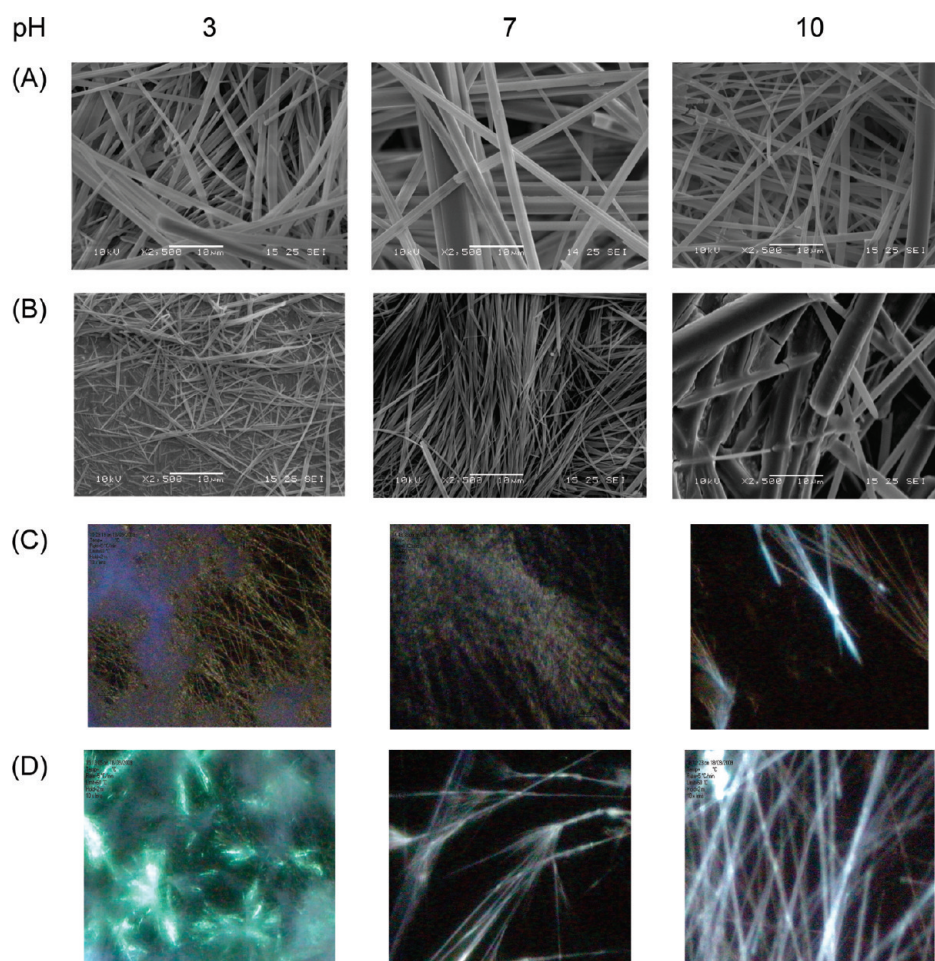


Figure 2. (A) SEM images of nanotubes formed at a pyrenyl moiety concentration of 0.002% m/m. (B) SEM images of nanotubes formed at a pyrenyl moiety concentration of 0.07% m/m. (C) EPM images (200 \times magnified) of samples with pyrenyl moiety concentrations of 0.002% m/m. (D) EPM images (200 \times magnified) of samples with pyrenyl moiety concentrations of 0.07% m/m. All images are of samples produced at distinct pH values.

morphological characteristics may be affected as well. SEM and EPM images were obtained for the samples produced at distinct pH values and are shown in Figure 2.

The data of the fluorophore-diluted samples in Figure 2A,C indicate that these materials are composed of 120 nm thick nanotubes that interact and are joined together to form fibrils. These fibrils are thicker when the systems are formed at neutral pH and are thinner at lower pH. At higher pH, fibrils are also formed by the interaction of thinner nanotubes, giving a final structure of 500–1300 nm that grows from the border of the substrate. At neutral pH, the obtained nanotubes are also long and interact with each other to generate fibrils that are 350–500 nm thick. The domains are formed in a radial structure, and their growth is limited by the encounter of two or more radial domains. At low pH, nanotubes are short and occur in subdomains that also grow radially. Additionally, many such subdomains can be found in the final structure. At high and neutral pHs, the delocalization of the fibril surface charges allows the fibrils to laterally self-assemble through hydrophobic interactions and to form large rigid ribbons when low fluorophore concentrations are present. A similar behavior was observed in the self-assembly process of Fmoc-diphenylalanine into fibrils.¹⁷

Fluorescence lifetimes were obtained for the samples at distinct pH ranges, and the data are summarized in Table 1.

All lifetimes are characteristic of pyrenyl groups, given that their values are in the hundreds of nanoseconds range. All curves show biexponential decays, which are explained by the presence of aggregates and/or excimers because these samples are in the solid phase and the nanotubes are very close to each other. This positioning makes possible, for example, the interaction between the pyrenyl adsorbed on the surface of two distinct nanotubes if one of them is close enough to the pyrenyl moiety adsorbed onto an adjacent nanotube. The shorter lifetimes are of tens of nanoseconds for all samples. It is noteworthy that the fluorescence lifetimes of the samples prepared at neutral pH are longer than those obtained at high and low pHs (see Table 1). This finding means that, at pH 7, the pyrenyl excited states are stabilized due to the interaction between the pyrenyl and the zwitterionic structures of the nanotube that only exist in this condition. The lifetime values obtained for the pH 3 and pH 10 samples are very similar. At these pH values, the protonated or deprotonated carboxyl structures of the pyrenyl and peptide moieties and the amino groups of the peptide termination do not lead to an excited structure that is as stable as that formed by the zwitterion at pH 7. These lifetime values are above 100 ns but are shorter than expected for free pyrenyl groups, which are reported to have lifetimes close to 400 ns.¹⁸ These results clearly show that pyrenyl moieties somehow interact with the peptide

Table 1. Fluorescence Lifetimes of Samples Produced at Distinct pH Values and Adsorbed onto Glass and ITO Surfaces

pH values	substrate	[pyrenyl/ peptide nanotubes], % m/m	τ_1	τ_2	χ^2
pH 3	glass	0.002	121 (± 3)	23 (± 7)	1.244
	ITO	0.002	129 (± 1)	17 (± 8)	1.188
	glass	0.07	107 (± 4)	19 (± 3)	1.144
	ITO	0.07	119 (± 2)	9 (± 5)	1.736
pH 7	glass	0.002	411 (± 12)	62 (± 1)	1.011
	ITO	0.002	234 (± 3)	29 (± 2)	1.089
	glass	0.07	348 (± 2)	68 (± 8)	1.131
	ITO	0.07	213 (± 8)	12 (± 5)	1.124
pH 10	glass	0.002	154 (± 1)	14 (± 1)	1.217
	ITO	0.002	113 (± 2)	11 (± 3)	1.140
	glass	0.07	126 (± 1)	17 (± 1)	1.112
	ITO	0.07	112 (± 1)	15 (± 4)	1.261

units, resulting in a shorter excited-state lifetime. These interactions must be of a Coulombic nature because they are determined by the charges present in both structures, which create an electrostatic force between these two compounds. The same behavior is observed when the fluorophore concentration is increased, although the lifetimes are quite short under this condition.

Effect of the Fluorophore Concentration. Two distinct pyrenyl concentrations were employed in the production of peptide nanotubes: 0.07% and 0.002% m/m of pyrenyl moieties/peptide. These concentration differences resulted in optical responses and structure changes at each pH that are dependent on the fluorophore concentration. These structural changes and the photophysical behavior are presented below. Figure 1 shows the fluorescence spectra obtained for both concentrations at each pH value. These data indicate that the vibronic structures from fluorescence spectra obtained for all diluted and concentrated samples are similar to those expected for pyrenyl-containing samples. There was no evidence of excimer or ground-state aggregation.

The SEM and EPM images shown in Figure 2 corroborate the effect of pyrenyl concentration on the organization of the nanotube structure. Figure 2 also shows that shorter and thinner nanotubes are obtained when the pyrenyl moiety concentration is increased at low and neutral pHs. On the other hand, thicker fibrils are obtained at higher pH, which implies that a balance between electrostatic and hydrophobic forces governs the fibril structure.

This result is exclusive to low fluorophore concentrations, and the thicker samples occur at neutral pH. As shown by Park et al.,⁴ the overall negative surface charge of these structures increases as the solution pH changes from acidic to alkaline. This change, according to the authors, leads to the disaggregation of the fibrils and to a smaller final structure. Furthermore, the overall negative charge is diminished at low pH, and fibrils are allowed to move closer to each other, giving thicker and longer final structures. This phenomenon is also found in the studied systems, but the negative surface charge is counterbalanced by the interaction with the fluorophore moieties in the nanotube formation environment. The final effect is, therefore, opposite to that described by Park⁴ and Tang,¹⁷ respectively. In these systems, longer and

thicker structures obtained at higher pH result in a greater overall negative charge on the fibril surfaces. This factor favors the π interaction between pyrenyl moieties and the peptide aromatic rings of the nanotubes, leading to a less charged nanotube surface, especially at higher pyrenyl concentrations. Thus, interactions between neighboring nanotubes are favored, and a major structure of larger and longer ribbons is formed. Given that the pK_a of 1-pyrene-carboxylic acid is 4.0¹⁹ at high pH, the carboxyl of the pyrenyl moieties are deprotonated. In addition, the ribbon surfaces present deprotonated carboxyl groups that form hydrogen bonds with water in solution and leave an overall negative charge over the surface structure that contributes to a more effective electrostatic interaction and to a more stabilized final structure. At low pH, however, pyrenyl moieties and peptide carboxyl groups are both protonated and the overall charge on the nanostructures is neutralized, which could lead to longer and larger fibrils, but the concentration of 1-pyrenyl-carboxylic acid moieties is high enough to evolve the structures and interact with them by π interactions with the peptide aromatic rings of the nanotubes. The interaction with water is diminished, the precipitation of the final structures occurs before their growth, and the obtained nanotubes are smaller. Finally, at neutral pH, $-NH_2$ terminal groups are protonated to $-NH_3^+$ and $-COOH$ terminal groups are deprotonated to $-COO^-$ to form the zwitterion. This zwitterion enables a more effective interaction between the formed structures and the water of the environment and favors the interaction with the deprotonated fluorophore carboxyl groups, resulting in a larger final structure. Furthermore, the inner portions of the isolated nanotubes are charged, favoring an electrostatic interaction with the fluorophore moieties. If this electrostatic force acts synergically with the π interactions that arise between those structures, intercalation of the pyrenyl moieties and the π -stacked diphenylalanine nanotubes' surface may occur. All of these assumptions are corroborated by quantum mechanical simulations, as presented in the dedicated section.

Substrate Interaction. Peptide nanotubes containing pyrenyl as a probe were formed over glass and ITO substrates. Fluorescence spectra and lifetimes were obtained, and the interaction between the substrate and the doped nanotubes was evaluated. Figure 3 presents the fluorescence spectra obtained from the samples deposited on ITO and glass.

Figure 3 shows that the spectra obtained from samples on ITO surfaces present a less vibronic structure at all pH values, but they present a shoulder at 374 nm, whereas in glass, spectra are red shifted and the maximum emission appears at 380 nm. This hypsochromic effect of the films deposited onto glass is expected because this solvent effect was observed for the pyrenyl derivative used in this work.²⁰ In addition, there is a hypsochromic effect because the solvent becomes more polar, indicating that the dipole momentum of the fluorophore is higher for the ground-state structure of the molecule than for the excited-state structure. This finding means that the specific interactions that occur when the material is adsorbed onto ITO are of the same nature as the polar–solvent interactions. Moreover, the intensity of the (0,0) band of emission of the pyrenyl moieties on ITO is diminished, indicating the possibility of an effective radioactive energy transfer between the fluorophore and the ITO surface. In addition, Mazur²¹ showed that pyrenyl units can be attached to ITO and that the optical response of this combination, when compared to material adsorbed on glass, is very similar to that described here with respect to peak intensities and hypsochromic shifts. The lifetime of the material on glass was also similar to those obtained

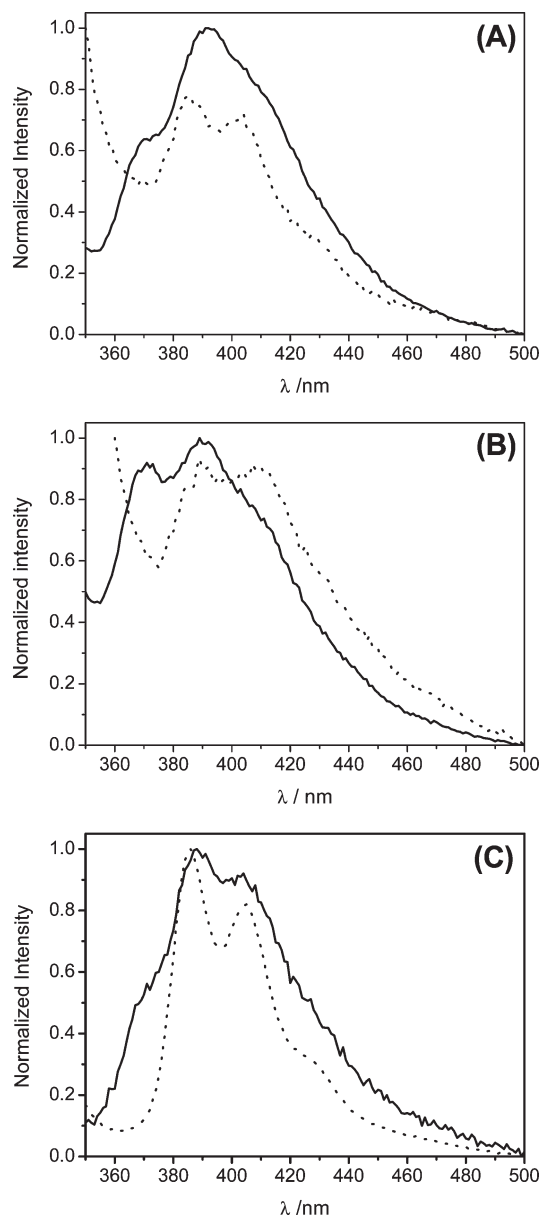


Figure 3. Fluorescence spectra of samples adsorbed on ITO (—) and glass (·····) substrates, produced at (A) pH = 3, (B) pH = 7, and (C) pH = 10.

here. However, the lifetime of the attached pyrenyl is very short compared with ours, and Mazur ascribes this finding to various processes, including singlet excited-state quenching by oxygen and Förster excitation transport.

To investigate our suggestion of a radiative energy transfer, fluorescence lifetimes were obtained for material adsorbed onto both glass and ITO, and the results are shown in Table 1. At neutral and high pHs, fluorescence lifetimes are shorter for samples adsorbed on ITO. At a higher pyrenyl concentration, this effect is also observed despite the general diminishing of the lifetimes.

These shorter lifetimes are due to radiative energy-transfer processes that occur between pyrenyl moieties on the peptide nanotubes and the ITO surface and corroborate the assumption based on the fluorescence spectra. These processes are facilitated by the peptide–ITO interaction of the dipole–induced dipole

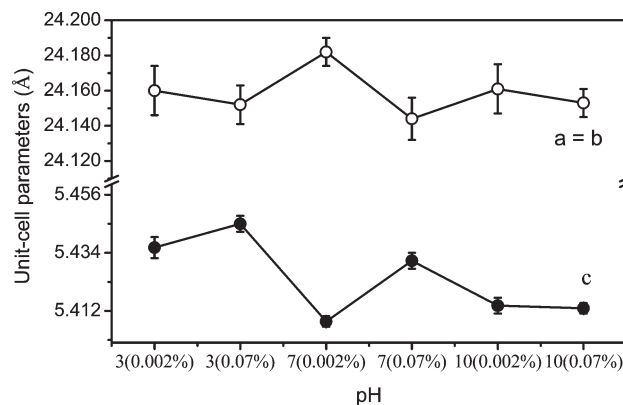


Figure 4. Unit cell parameters obtained from DRX patterns of nanotube samples produced at distinct pH ranges and pyrenyl concentrations.

type. In fact, there is a very strong interaction between these species, as demonstrated by Lee,²² who obtained ITO particles with enhanced properties by growing them into self-assembled peptide-derivative structures, thus permitting control of the shape and the crystalline structure of the ITO particles formed.

X-ray Diffraction and Computational Results. To obtain information regarding the conformational change that the fluorophore concentration may cause to the primer nanotube, X-ray diffractograms were recorded. Unit cell parameters were obtained from Rietveld refinements (not shown) of the nanotube phase only (the phase of the ITO coating was not included), considering the structural model described by Kim et al.¹⁴ With this goal, the General Structure Analysis System (GSAS)²³ software program and its graphical user interface, EXPGUI,²⁴ were used. Neither the fractional coordinates nor the atomic displacement parameters were varied during refinements. The background was fitted using a 20-term Chebyshev polynomial. As shown in Figure 4, the unit cell parameters present a slight decreasing trend at distinct pH ranges when considering samples produced at higher fluorophore concentrations. Although the unit cell parameters *a* and *b* are equivalent for nanotubes prepared at distinct pH ranges and constant even when the fluorophore concentration changes, the unit cell parameter *c* decreases as the pH increases and is constant when the fluorophore concentration changes at high pH. At low and neutral pHs, the unit cell parameter *c* increases as the fluorophore concentration is increased, even though this effect is much more pronounced at neutral pH.

Because the interaction between the nanotube walls and fluorophore moieties occurs via interacting forces that describe the balance between Coulombic, π -stacking, and van der Waals contributions, it is expected that fluorophore moieties can be found at low and neutral pHs between the nanotube hexagonal lamellae indexed as belonging to the $P6_1$ space group, as described by Kim.¹⁴ The more pronounced effect at neutral pH is due to more effective π -stacking and Coulombic interactions because the terminal groups of both the fluorophore and the nanotubes are deprotonated at this pH. For nanotubes produced at high pH, the parameter *c* is constant, as expected, because they are close enough to one another to form ribbons, and this effect contributes to a minor insertion of the fluorophores into the hexagonal structures. This result also corroborates a previous work of our research group.²⁵

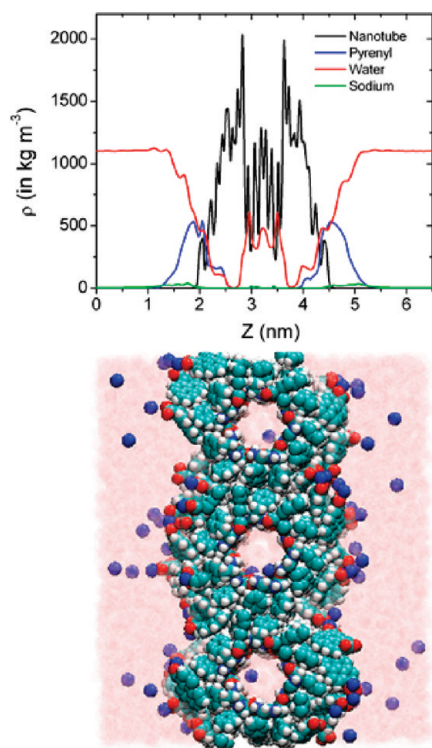


Figure 5. Mass-density distribution (kg m^{-3}) computed for the components of the ionic system and a representative view of a configuration. The density of the fluid phase from the nanotube surface varies considerably along the z direction.

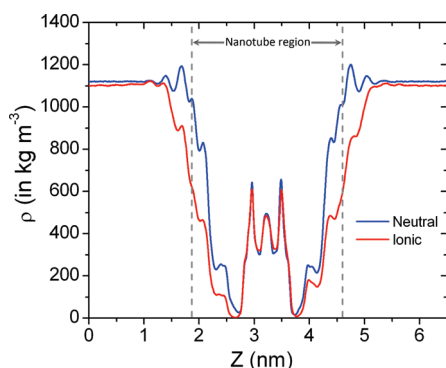


Figure 6. Comparison between water mass-density distributions (kg m^{-3}) computed for the ionic and neutral systems.

As can be seen in Figures 2 and 3, the nanotubes formed at high pH show a highly efficient fluorescence, which, along with the fact that the c axis does not suffer any considerable variation at this pH range, indicates that the fluorophore is adsorbed to the nanotube surface. This kind of interaction was previously studied by Ramasamy et al.²⁶

The main concern herein was to understand the interfacial properties of the interaction between the fluorophore and nanotube surfaces and to determine the nature of the functionalization. From the NPT conditions, simulations of structural and dynamic properties of the nanotube aqueous solutions after 8 ns were analyzed. Figures 5 and 6 show the mass-density profiles (along the z direction) for the components of the ionic system and an atomistic representation of the system. It is noteworthy

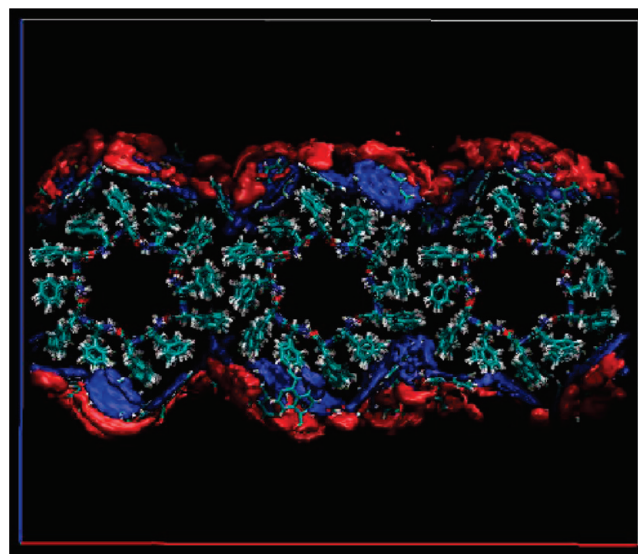


Figure 7. Spatial distribution function of pyrenyl hydrophilic (in red) and hydrophobic (in blue) groups. The surface has been drawn at an isovalue of 9, which is 4 times the average number density of pyrenyl molecules.

that the water profile does not present a pronounced peak near the nanotube surface. Instead, the density increases smoothly from the surface, revealing the soft character of the nanotube. Inside the tube, a larger structuring of water molecules is found to interact with the inner wall, showing a clear confinement pattern with a hydration shell near the internal surface and a peak concentration on the nanotube axis.

As shown in earlier sections, aromatic rings are expected to show a strong attractive interaction with the hydrophobic surface of the nanotube and play an important role in providing effective adhesion of the pyrenyl ions. In fact, the mass-density profile of the ionic components indicates that the pyrenyl ions are adsorbed on the nanotube surface, which corroborates the experimental findings.

A better visualization of the three-dimensional local adsorption structure can be obtained from the spatial distribution function of the pyrenyl near the nanotube surface (Figure 7). From Figure 7, pyrenyl moieties (in red and blue) near the surface tend to spread isotropically, and the spatial distribution of pyrenyl molecules appears highly localized, suggesting that the molecule remains in the position in which it was adsorbed.

A similar analysis based on the spatial distribution of hydrophilic and hydrophobic groups indicates a preferential orientation in the adsorption process. As shown in Figure 7, the hydrophilic head ($-\text{COO}^-$, in red) tends to point to the bulk water, while the hydrophobic part (in blue) remains attached to the surface of the tube. This result suggests that it is possible to functionalize the nanotube by adsorption of aromatic ions on its surface. The results of the dynamics of the system support this functionalization and are discussed in the Supporting Information.

CONCLUSION

L-Phe \cdots L-Phe peptide nanotubes were produced using distinct synthesis conditions, including pH and fluorophore concentrations. These conditions were found to play an important

role in determining the final structure of the material. Changes in pH yield final fibrils of different forms because they can assume the form of ribbons (increased pH) or wires (decreased pH) and different lengths (longer fibrils are obtained at higher pH values). Furthermore, the fluorophore concentration interferes with the final structure, retarding the nanotube growth at low pH by leading to antagonist interaction forces between nanotube-forming units and favoring growth at higher pH values by contributing to synergic forces of interaction. XRD measurements reveal that the insertion of fluorophore moieties between hexagonal lamellae that form the primary structure of the nanotube occurs at low and neutral pHs and is greatly favored at neutral pH and higher fluorophore concentrations. Computational simulations were performed to investigate the characteristics of the adsorption mechanisms and the nature and balance of the interactions that lead to the final structure. These simulations show that the nanotube formation and adsorption processes are governed mainly by π -stacking interactions and that electrostatic interactions are essential to the functionalization of these materials, which is in agreement with experimental findings. The produced materials were deposited onto glass and ITO-covered glass substrates, and radiative energy-transfer processes between fluorophore moieties and the ITO substrate were suggested by fluorescence spectra and fluorescence lifetime measurements. This finding could be useful for electronic applications.

■ ASSOCIATED CONTENT

Supporting Information. Computational details and fluorescence lifetimes curves. This material is available free of charge via the Internet at <http://pubs.acs.org>.

■ AUTHOR INFORMATION

Corresponding Author

*E-mail: wendel.alves@ufabc.edu.br.

■ ACKNOWLEDGMENT

Financial support by the Brazilian agencies Fundação de Amparo à Pesquisa do Estado de São Paulo (FAPESP, Grant No. 08/53576-9) is gratefully acknowledged. This work was also supported by INCT in Bioanalytics (FAPESP, Grant No. 08/57805-2 and CNPq, Grant No. 573672/2008-3). We are thankful to LME-LNLS (Project SEM-LV 9004 and SEM-FEG 8511), and we also thank Professor Teresa Atvars and the University of Campinas for the use of the fluorescence microscope and spectrophotometers.

■ REFERENCES

- (1) Ghadiri, M. R.; Granja, J. R.; Milligan, R. A.; McRee, D. E.; Khazanovich, N. *Nature* **1993**, 366, 324.
- (2) (a) Whitesides, G. M.; Mathias, J. P.; Seto, C. T. *Science* **1991**, 254, 1312. (b) Zhang, S. *Nat. Biotechnol.* **2003**, 21, 1171. (c) Reches, M.; Gazit, E. *Curr. Nanosci.* **2006**, 2, 105. (d) Whitesides, G. M.; Grzybowski, B. *Science* **2002**, 295, 2418. (e) Hamelin, B.; Jullien, L.; Derouet, C.; duPenhoat, C. H.; Berthault, P. *J. Am. Chem. Soc.* **1998**, 120, 8438. (f) Reches, M.; Gazit, E. *Science* **2003**, 300, 625.
- (3) (a) Han, T. H.; Ok, T.; Kim, J.; Shin, D. O.; Ihee, H.; Lee, H.-S.; Kim, S. O. *Small* **2010**, 6, 945. (b) Han, T. H.; Kim, J.; Park, J. S.; Park, C. B.; Ihee, H.; Kim, S. O. *Adv. Mater.* **2007**, 19, 3924. (c) Lee, J. S.; Yoon, I.; Kim, J.; Ihee, H.; Kim, B.; Park, C. B. *Angew. Chem., Int. Ed.* **2011**, 50, 1164. (d) Han, T. H.; Oh, J. K.; Lee, G.-J.; Pyun, S. I.;

- Kim, S. O. *Colloids Surf., B* **2010**, 79, 440. (e) Menzenski, M. Z.; Banerjee, I. A. *New J. Chem.* **2007**, 31, 1674. (f) Shimizu, T.; Masuda, M.; Minamikawa, H. *Chem. Rev.* **2005**, 105, 1401.
- (4) Park, J. S.; Han, T. H.; Oh, J. K.; Kim, S. O. *Macromol. Chem. Phys.* **2009**, 210, 1283.
- (5) Buriak, J. M.; Ghadiri, M. R. *Mater. Sci. Eng., C* **1997**, 4, 207.
- (6) Riley, J. M.; Aggeli, A.; Koopmans, R. J.; McPherson, M. J. *Biotechnol. Bioeng.* **2009**, 103, 241.
- (7) Rughani, R. V.; Salick, D. A.; Lamm, M. S.; Yucel, T.; Pochan, D. J.; Schneider, J. P. *Biomacromolecules* **2009**, 10, 1295.
- (8) (a) Liang, Y.; Guo, P.; Pingali, S. V.; Pabir, S.; Thiagarajan, P.; Berland, K. M.; Lynn, D. G. *Chem. Commun.* **2008**, 6522. (b) Heinze, K.; Hempel, K. *Chem.—Eur. J.* **2009**, 15, 1346. (c) Kuciauskas, D.; Caputo, G. A. *J. Phys. Chem. B* **2009**, 113, 14439. (d) Channon, K. J.; Devlin, G. L.; MacPhee, C. E. *J. Am. Chem. Soc.* **2009**, 131, 12520.
- (9) Synytsya, A.; Synytsya, A.; Blafkova, P.; Ederova, J.; Spevacek, J.; Slepicka, P.; Kra, V.; Volka, K. *Biomacromolecules* **2009**, 10, 1067.
- (10) (a) Meyers, S. R.; Khoo, X. J.; Huang, X.; Walsh, E. B.; Grinstaff, M. W.; Kenan, D. J. *Biomaterials* **2009**, 30, 277. (b) Nygren, P.; Lundqvist, M.; Liedberg, B.; Jonsson, B. H.; Ederth, T. *Langmuir* **2010**, 26, 6437. (c) Gazit, E. *Chem. Soc. Rev.* **2007**, 36, 1263.
- (11) Channon, K. J.; Devlin, G. L.; Magennis, S. W.; Finlayson, C. E.; Tickler, A. K.; Silva, C.; MacPhee, C. E. *J. Am. Chem. Soc.* **2008**, 130, 5487.
- (12) (a) Jayawarna, V.; Ali, M.; Jowitt, T. A.; Miller, A. F.; Saiani, A.; Gough, J. E.; Ulijn, R. V. *Adv. Mater.* **2006**, 18, 611. (b) Zhang, Y.; Gu, H.; Yang, Z.; Xu, B. *J. Am. Chem. Soc.* **2003**, 125, 13680.
- (13) (a) Gorbitz, C. H. *Chem. Commun.* **2006**, 2332. (b) Gorbitz, C. H. *Chem.—Eur. J.* **2001**, 7, 5153.
- (14) Kim, J.; Han, T. H.; Kim, Y. I.; Park, J. S.; Choi, J.; Churchill, D. G.; Kim, S. O.; Ihee, H. *Adv. Mater.* **2010**, 22, 583.
- (15) Hess, B.; Kutzner, C.; van der Spoel, D.; Lindahl, E. *J. Chem. Theory Comput.* **2008**, 4, 435.
- (16) MacKerell, A. D., Jr.; Bashford, D.; Bellott, R. L.; Dunbrack, R. L., Jr.; Evanseck, J. D.; Field, M. J.; Fischer, S.; Gao, J.; Guo, H.; Ha, S.; Joseph-McCarthy, D.; Kuchnir, L.; Kucera, K.; Lau, F. T. K.; Mattos, C.; Michnick, S.; Ngo, T.; Nguyen, D. T.; Prodhom, B.; Reiher, W. E., III; Roux, B.; Schlenkrich, M.; Smith, J. C.; Stote, R.; Straub, J.; Watanabe, M.; Wiorkiewicz-Kuczera, J.; Yin, D.; Karplus, M. *J. Phys. Chem.* **1998**, 102, 3586.
- (17) Tang, C.; Smith, A. M.; Collins, R. F.; Ulijn, R. V.; Saiani, A. *Langmuir* **2009**, 25, 9447.
- (18) Kósa, C.; Danko, M.; Fiedlerová, A.; Hrdlovic, P.; Borsig, E.; Weiss, R. G. *Macromolecules* **2001**, 34, 2673.
- (19) Donckt, E.; Dramaix, J.; Nasielski, J.; Vogels, C. *Trans. Faraday Soc.* **1969**, 65, 3258–3262.
- (20) Birks, J. B. *Photophysics of Aromatic Molecules*; Wiley: London, U.K., 1970.
- (21) Mazur, M.; Blanchard, G. J. *Bioelectrochemistry* **2005**, 66, 89–94.
- (22) Lee, I.; Lee, S. Y. *J. Phys. Chem. C* **2009**, 113, 17372.
- (23) Larson, A. C.; Von Dreele, R. B. *General Structure Analysis System (GSAS)*; Report LAUR 86-748; Los Alamos National Laboratory: Los Alamos National Laboratory: Los Alamos, NM, 1994.
- (24) Toby, B. H. *J. Appl. Crystallogr.* **2001**, 34, 210.
- (25) Cipriano, T. C.; Takahashi, P. M.; de Lima, D.; Oliveira, V. X., Jr.; Souza, J. A.; Martinho, H.; Alves, W. A. J. *Mater. Sci.* **2010**, 45, S101.
- (26) Ramasamy, R. P.; Luckarift, H. R.; Ivnikski, D. M.; Atanassov, P. B.; Johnson, G. R. *Chem. Commun.* **2010**, 46, 6045.